A QUANTITATIVE DISCRETE ELEMENT MODEL TO INVESTIGATE SUB-SURFACE DAMAGE DUE TO SURFACE POLISHING

Damien André, Ivan Iordanoff, Jean-Luc Charles, Jérôme Néauport

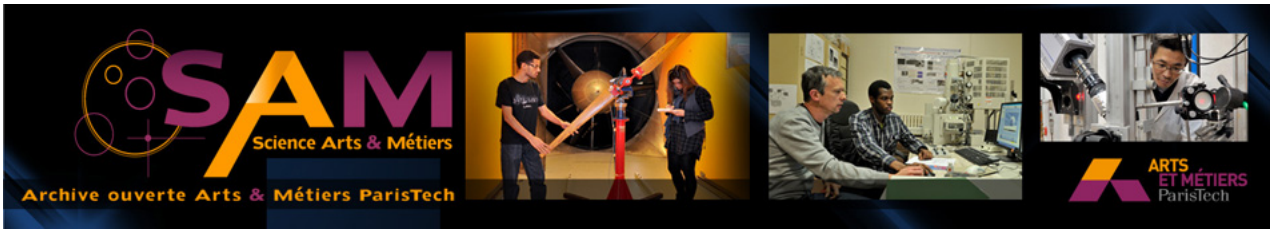

A QUANTITATIVE DISCRETE ELEMENT MODEL TO INVESTIGATE SUB-SURFACE DAMAGE DUE TO SURFACE POLISHING

Damien André
Arts & Métiers ParisTech,
I2M-DuMAS, UMR 5295 CNRS,
F-33405, Talence, France
Email: damien.andre@etu.u-bordeaux1.fr

Ivan Iordanoff
Second Coauthor
Arts & Métiers ParisTech,
I2M-DuMAS, UMR 5295 CNRS,
F-33405, Talence, France
Email: ivan.iordanoff@ensam.eu

Jean-luc Charles
third Coauthor
Arts & Métiers ParisTech,
I2M-DuMAS, UMR 5295 CNRS,
F-33405, Talence, France
Email: j.charles@i2m.u-bordeaux1.fr

Jérôme Néauport
fourth Coauthor
Commissariat à l'Énergie Atomique,
Centre d'Études Scientif ques et Techniques d'Aquitaine,
F-33114 Le Barp, France
Email: jerome.neauport@projet-lmj.org

ABSTRACT

This work is a continuation of a previous study that investigated sub-surface damage in silica glass due to surface polishing. In this previous study, discrete element models have shown qualitatively good agreement with experiments. The presented work propose a model allowing quantitative results by focusing on the continuous part of the problem. Special attemption was given to the discrete element model of silica glass considered as perfectly isotropic, elastic and brittle. To validate this approach, numerical results are compared to experimental data from literature.

Introduction

When fused silica optics are submitted to high-power laser (such as megajoule laser or National Ignition Facility) at the wavelength of 351 nm, fused silica optics can exhibit damage, induced by the high amount of energy traversing the part [1]. Current researches have shown that this damage could be initiated on pre-existing Sub-Surface Damages (SSD) created during the polishing processes [2–7]. The discrete element method (DEM) is proposed to simulate the polishing process and its impact on sub-surface damage creation.

Discrete element model is well adapted to simulate a media that has a great number of interfaces. It has been widely used to study tribological problems like wear phenomena [8–14]. In this kind of problem, the material has a continuous part (the volume above the surface that is not yet affected by the wear), a continuous part with cracks (called sub-surface damage in abrasion process terminology) and a discontinuous part (the interfacial media, called third body, that is a mixture of abrasive particles and wear particles). Discrete element model must be able to simulate with accuracy all these parts of the material.

This work is a continuation of a previous study that investigated sub-surface damage in silica glass due to surface polishing [15]. In this previous study, discrete element models have shown qualitatively good agreement with experiments. The presented work propose a model allowing quantitative results by fo-

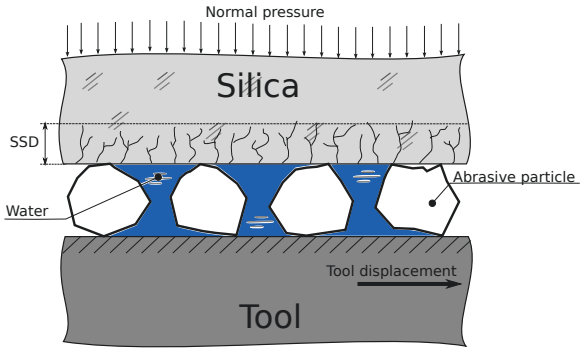

FIGURE 1: Loose abrasive grinding principle

cusing on the continuous part of the problem. Special attemption was given to the discrete element model of silica glass considered as perfectly isotropic, elastic and brittle. To validate this approach, numerical results are compared to experimental data from literature.

Loose abrasive grinding

This work focuses on the polishing step called *loose abrasive grinding*. Figure 1 shows the principle of loose abrasive grinding. The silica is subjected to a vertical pressure and the tool moves horizontally. The grinding interface is composed by abrasive particle in suspension into a water solution : the slurry. This process causes scratches and digs inside the silica layer. These cracks take part in the abrasion process but some of them subsist in a thin layer and give the subsurface damage zone.

Numerical model

Integration scheme

The numerical resolution is based on an explicit integration scheme well adapted to massive DEM simulation [16] and high velocity phenomena such as fracturing or impact simulation. Many explicit schemes can be used : the Verlet velocity, Runge-Kutta, leapfrog or gear's method... [17, §13]. In reference [16], the authors have compared these algorithms *"in terms of accuracy, stability and CPU eff ciency"*. It appears that all of them give approximately the same eff ciency.

Velocity Verlet scheme is chosen for its simplicity . Discrete element position and velocity are estimated by:

$$\vec{p}(t+dt) = \vec{p}(t) + dt\,\vec{p}(t) + \frac{dt^2}{2}\vec{\ddot{p}}(t) \tag{1}$$

$$\vec{\dot{p}}(t+dt) = \vec{\dot{p}}(t) + \frac{dt}{2}\left(\vec{\ddot{p}}(t) + \vec{\ddot{p}}(t+dt)\right) \tag{2}$$

where :

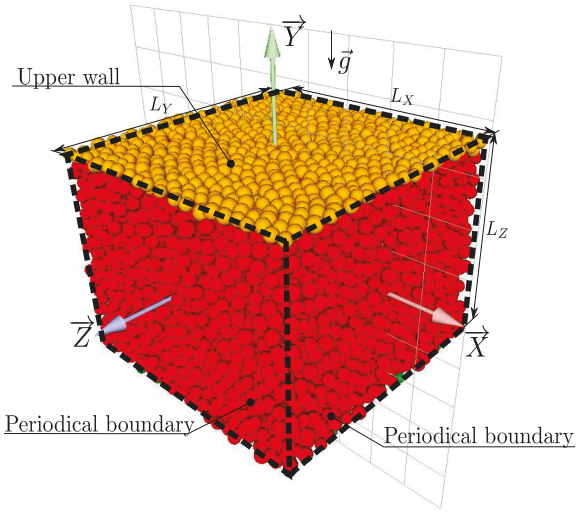

FIGURE 2: The silica cube

t is the current time and dt is the integration time step.
$p(t)$, $\dot{p}(t)$ and $\ddot{p}(t)$ is the discrete element linear position, velocity and acceleration.

The discrete element orientations are described by quaternions, noted $q(t)$, that allow an eff ciency way to compute the rotation of the local frames associated with discrete elements [18, §2.5]. The velocity Verlet scheme is also applied to quaternion $q(t)$, with:

$$q(t+dt) = q(t) + dt\,\dot{q}(t) + \frac{dt^2}{2}\ddot{q}(t) \tag{3}$$

$$\dot{q}(t+dt) = \dot{q}(t) + \frac{dt}{2}\left(\ddot{q}(t) + \ddot{q}(t+dt)\right) \tag{4}$$

Geometrical description

According to f gure 2, the silica piece to be surfaced is constituted by spheres linked together by elastic solid joints. This cluster form a cube with a dimension of 150 μm. This dimension is chosen according to the maximal SSD length experimentally observed. The average silica discrete element radius is around 4.7 μm to keep reasonable computational duration. The radius of a given sphere is chosen randomly around this mean value. The tool is simply def ned by an elastic plane. The abrasive particles are placed between the silica cube and the tool (see f gure 3).

Boundary conditions

The upper wall have a single degree of freedom that allows translation on the $\vec{Y}$ axis. An unidirectional condition is also imposed. The upper wall can only go down. Additionally, a normal

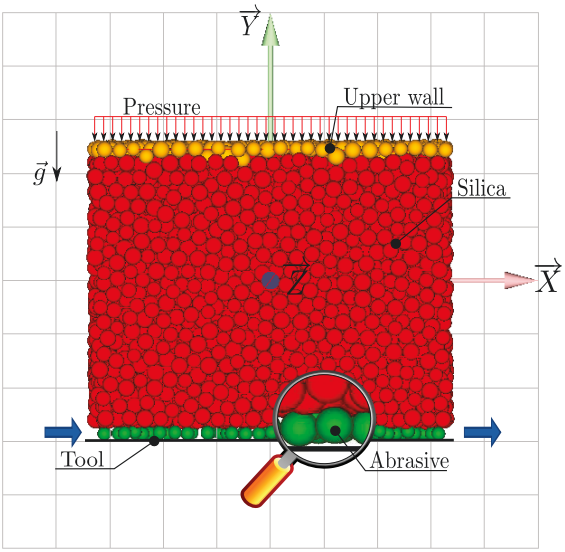

FIGURE 3: Global view of model

pressure along $-\vec{Y}$ axis is applied on the upper wall. A velocity condition is imposed to the abrasive particles : they are constrained to move along the $\vec{X}$ axis with a velocity equal to the tool velocity. Periodical boundary conditions are applied on the sides in order to mimic an inf nite f ow f eld along $\vec{X}$ and $\vec{Z}$.

The silica model

The silica is considered as a brittle elastic material. The discrete element belonged to the silica cube are linked by elastic Euler-Bernouilli beams which produce more realistic crack pattern than the simple spring model or the dual spring model [19, 20, §3].

Cohesive beam bond model The cylindrical geometry is chosen because it's dimensional description requires only two independent parameters: a length L_μ and a radius r_μ[1]. The mechanical properties are also linked to the cohesive beams: a Young's modulus E_μ and a Poisson's ratio ν_μ. These four geometric and mechanical parameters suff ce to describe the cohesive beam. Note that the cohesive beams are mass-less; mass properties are assigned only to the discrete elements.

For the sake of clarity f gure 4 shows a conf guration in which the discrete elements have been moved away. The cohesive beam is symbolized by its median line. Both cohesive bond ends are f xed to the discrete element centers O_1 and O_2. Figure 4b shows the cohesive beam in a loading state induced by the discrete element movement relatively to the initial conf guration.

[1]To distinguish micro from macro properties, micro parameters are denoted by 'μ' and macro parameters by 'M'.

The analytic model of Euler-Bernoulli beam is well known [21]. In reference [22, §6.2], the author describe a stiffness matrix expressed in the beam local frame for a f nite element application. Consequently, the force and torque reactions acting on discrete elements 1 and 2 are:

$$\overrightarrow{F_{DE1}} = +E_\mu S_\mu \frac{\Delta l_\mu}{l_\mu}\vec{X} - \frac{6E_\mu I_\mu}{l_\mu^2}\left((\theta_{2z}+\theta_{1z})\vec{Y} + (\theta_{2y}+\theta_{1y})\vec{Z}\right) \quad (5)$$

$$\overrightarrow{F_{DE2}} = -E_\mu S_\mu \frac{\Delta l_\mu}{l_\mu}\vec{X} + \frac{6E_\mu I_\mu}{l_\mu^2}\left((\theta_{2z}+\theta_{1z})\vec{Y} - (\theta_{2y}+\theta_{1y})\vec{Z}\right) \quad (6)$$

$$\overrightarrow{T_{DE1}} = +\frac{G_\mu Io_\mu}{l_\mu}(\theta_{2x}-\theta_{1x})\vec{X} - \frac{2E_\mu I_\mu}{l_\mu}\left((\theta_{2y}+2\theta_{1y})\vec{Y} - (\theta_{2z}+2\theta_{1z})\vec{Z}\right) \quad (7)$$

$$\overrightarrow{T_{DE2}} = -\frac{G_\mu Io_\mu}{l_\mu}(\theta_{2x}-\theta_{1x})\vec{X} - \frac{2E_\mu I_\mu}{l_\mu}\left((2\theta_{2y}+\theta_{1y})\vec{Y} - (2\theta_{2z}+\theta_{1z})\vec{Z}\right) \quad (8)$$

where:

$\overrightarrow{F_{DE1}}$ and $\overrightarrow{F_{DE2}}$ are the beam force reactions acting on discrete elements 1 and 2.

$\overrightarrow{T_{DE1}}$ and $\overrightarrow{T_{DE2}}$ are the beam torque reactions acting on discrete elements 1 and 2.

l_μ and Δl_μ are the initial beam length and the longitudinal extension.

$\vec{\theta_1}(\theta_{1x},\theta_{1y},\theta_{1z})$ and $\vec{\theta_2}(\theta_{2x},\theta_{2y},\theta_{2z})$ are the rotations of beam cross section at the points O_1 and O_2 expressed in the beam local frame.

S_μ, Io_μ and I_μ are the beam cross section area, polar moment of inertia and moment of inertia along $\vec{Y}$ and $\vec{Z}$.

E_μ and G_μ are the Young and shear modulus.

Note that reaction force and torque are expressed in the beam local frame F. The four parameters that def ne the micro beam, L_μ, r_μ, E_μ and ν_μ have only an inf uence on the elastic behavior of the assembly. These microscopic parameters are calibrated thanks to tensile tests to produce at the macroscopic level the silica Young modulus and Poisson ratio.

A failure criterion is introduce to mimic cracks inside the silica. This criterion is based on material strength theory of brittle

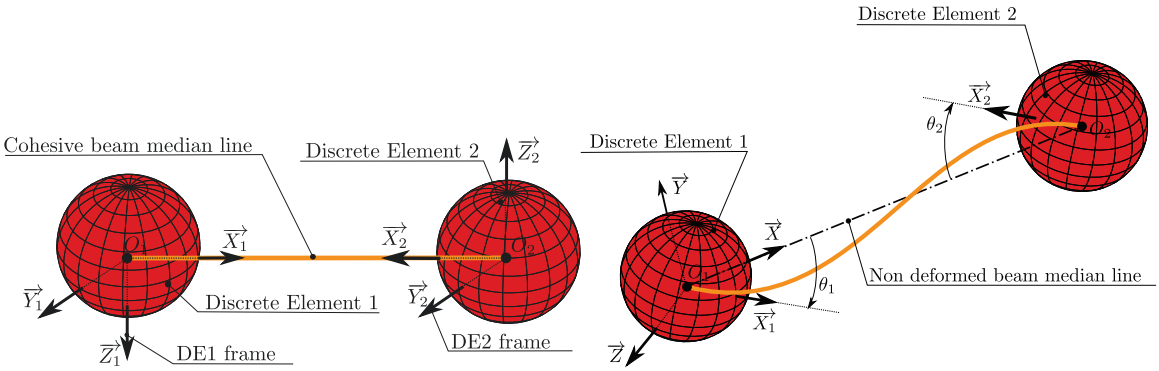

(a) Relaxing state (b) Loading state

FIGURE 4: Cohesive beam bond conf guration

material :

$$\sigma_{\mu_f} \geq \frac{1}{2}\left(\sigma_{\mu_{max}} + \sqrt{\sigma^2_{\mu_{max}} + 4\tau^2_{\mu_{max}}}\right) \tag{9}$$

The stress criterion σ_{μ_f} is also calibrated thanks to tensile failure tests.

The silica contact model After a beam failure, the discrete elements linked by a broken beam could interact by elastic contact. To deduce the contact stiffness, virtual semi-cubic shapes, $\mathscr{C}_1$ and $\mathscr{C}_2$, are associated to discrete elements (see f gure 5). This process allows to correct the residual void between spherical discrete element. The contact stiffness is :

$$K = 4E\frac{R_1 R_2}{R_1 + R_2} \tag{10}$$

Where E is the silica Young modulus and R_1 and R_2 are the discrete element radii.

Hertzian contact

Except the silica discrete elements that model a single body, all the other discrete elements, that model distinct body, could interact by contacts. The shape of these discrete elements are supposed representative of their real morphology. The contact law between distinct body are deduced from the hertzian contact model between two spheres:

$$\vec{f} = \frac{4}{3}E^*\delta\sqrt{\frac{R_1 R_2}{R_1 + R_2}\delta}\,\vec{n} \tag{11}$$

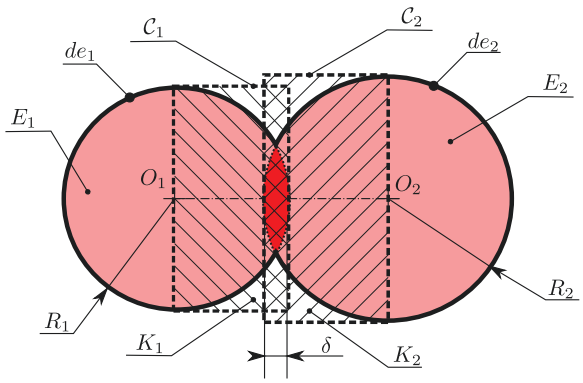

FIGURE 5: The contact model between two discrete element silica

With:

$$E^* = \frac{E_1(1-\nu_2^2) + E_2(1-\nu_1^2)}{E_1 E_2} \tag{12}$$

Where $\vec{f}$ is the reaction force, E_1, E_2, ν_2, ν_2 the body's Young modulus and Poisson ratio, δ the sphere interpenetration, and $\vec{n}$ a unit vector along the contact normal direction.

The f uid model

The water solution during the grinding process is considered as a Couette f ow. The f uid velocity is characterized by a linear gradient inside its thickness. At the interface, the maximal and minimal velocity are equal to the tool velocity and the silica velocity (considered as null) (see f gure 6). The action of the f uid

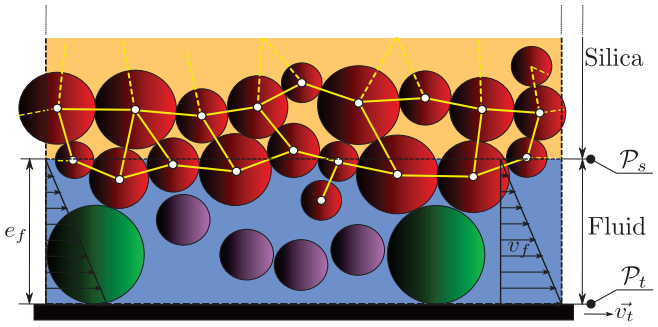

FIGURE 6: 2D illustration of the f uid model

acting on submerged discrete element are given by [23, §7.4]:

$$\vec{f} = 8\pi\eta R(\vec{v_f} - \vec{v_d}) \tag{13}$$

$$\vec{m} = 8\pi\eta R^3(\vec{\omega_f} - \vec{\omega_d}) \tag{14}$$

Where:

η is the f uid viscosity.
R is the discrete element radius.
$\vec{v_f}$ and $\vec{\omega_f}$ are linear and angular f uid velocities computed at the discrete element altitude.
$\vec{v_d}$ and $\vec{\omega_d}$ are linear and angular discrete element velocities.

The linear and angular f uid velocities for a given altitude y_d are given by:

$$\vec{v_f} = \|\vec{v_t}\| \left(1 - \frac{y_d}{e_f}\right) \vec{X} \tag{15}$$

$$\vec{\omega_f} = \frac{\|\vec{v_t}\|}{e_f} \vec{Z} \tag{16}$$

Subsurface damage measurement method

For optic manufacturers the main interesting value is the maximal SSD length that characterize their process. In the DEM model, it is considered that a broken beam inside the silica cube model a SSD. The length of this SSD is given by the altitude of the broken beam in relation to the ”abraded surface” of the silica.

The abraded surface is considered as the last silica discrete element layer (in contact with the slurry). During the simulation, the morphology of this layer changes. An algorithm is used to update and save the positions of discrete elements belonging to this layer. This position set is treated by linear interpolation to reach a 3D map of the abraded surface $\mathscr{S}$ (see f gure 7).

The SSD length is computed by projected the broken beam position (red circle points on the f gure) on the interpolated surface $\mathscr{S}$ along the $-\vec{Y}$ axis (blue square points on the f gure).

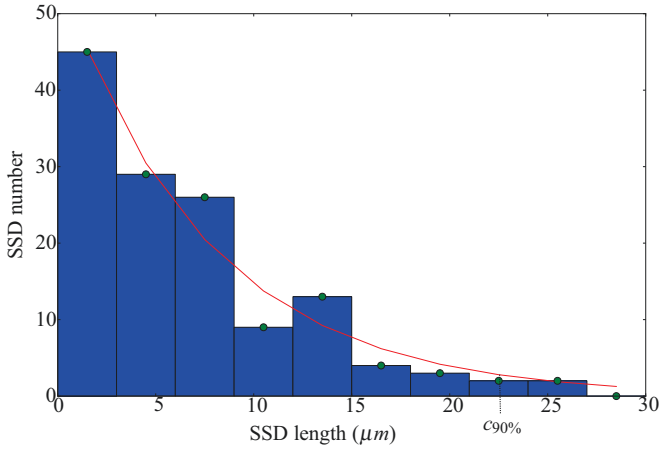

FIGURE 8: SSD distribution as a function of their length

Finally, the SSD length, noted c_{SSD}, is given by the distance between these two positions.

This numerical treatment allows to plot an histogram of the SSD number as a function of their lengths (see f gure 8). This distribution shows good agreement with experimental observations [24] and could be approximated by a decreasing exponential function :

$$f(x) = ae^{-bx} \qquad \text{with} \quad b \geq 0 \tag{17}$$

The a and b coeff cient are f tted by a least square method (see red curve on f gure 8). They allow to compute a criterion based on statistical assumption. It is considered that the maximal SSD length is the length where 90% of SSD are below this value. This value is noted $c_{90\%}$.

The f gure 9 shows the evolution of $c_{90\%}$ during the simulation. It is observed that, after a delay, the value becomes stable. This converged value is considered as representative of the maximal length of SSD for a given numerical experience.

Numerical experiences

The experimental observation given by ref. [25] are taken as reference of this study. The numerical boundary conditions and loading are calibrated to f t with the experimental process. The inf uence of abrasive particle size, tool velocity and concentration are studied.

To reach this goal an experience with average values of these parameters is taken as reference. For a given experience only one parameter is studied. The table 1 summarizes the numerical experiences and their parameter values. The values are expressed in two ways : the experimental way (column **exp**) and the numerical model way (column **dem**). In this table, the ’-’ character

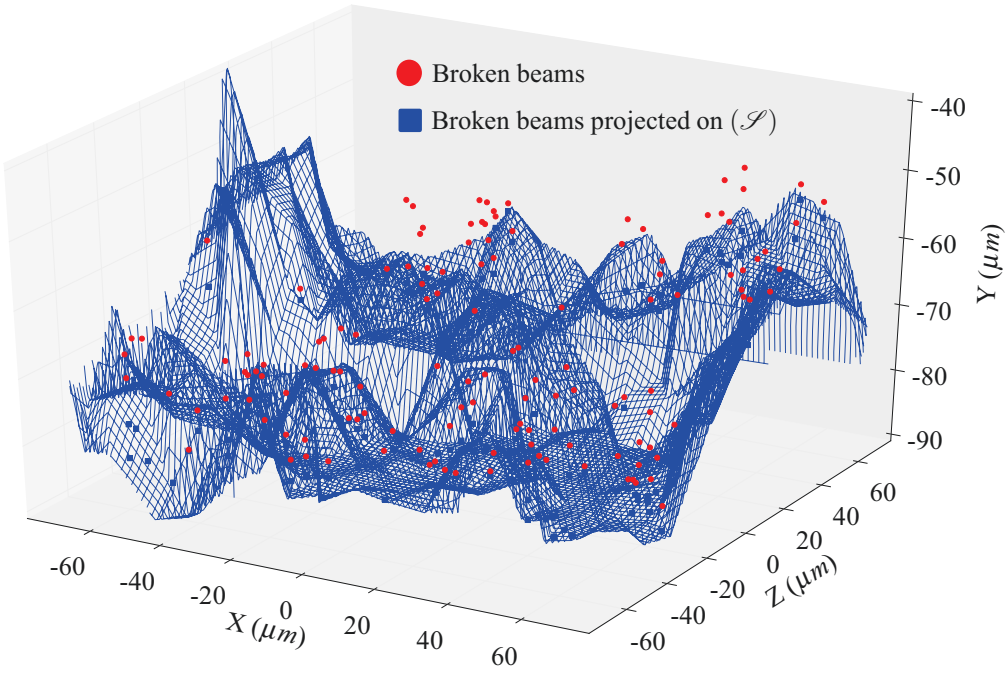

FIGURE 7: 3D map of the abraded surface and SSD length

Exp. Name	**Parameters**							
	pressure		tool velocity		abrasive size		concentration	
	exp	**dem**	**exp**	**dem**	**exp**	**dem**	**exp**	**dem**
	Kg	mN	rpm	$m.s^{-1}$	μm	μm	%	(*)
reference	1.6	0.18	15	0.24	10	10	6	7
velocity[1] -	-	-	5	0.08	-	-	-	-
velocity[1] +	-	-	25	0.40	-	-	-	-
radius[2] -	-	-	-	-	5	5	-	-
radius[2] +	-	-	-	-	15	15	-	-
concentration[3] +	-	-	-	-	-	-	12	13
concentration[3] ++	-	-	-	-	-	-	18	19

(*): abrasive number

1: more precisely the tool velocity

2: more precisely the abrasive radius

3: more precisely the abrasive concentration of the slurry

TABLE 1: Summary of numerical experiences with their parameter values

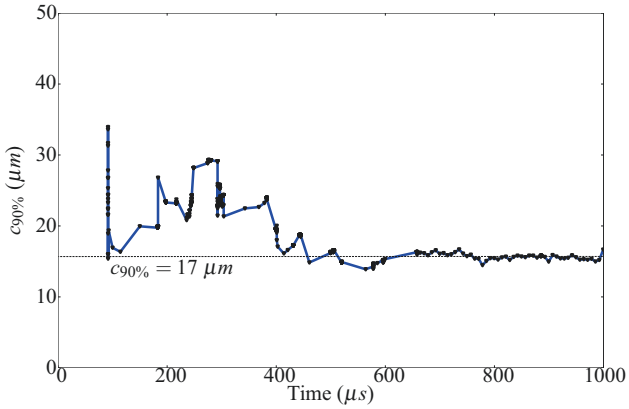

FIGURE 9: SSD max evolution

means that the given parameter have the same value that the reference numerical experience.

Results and discussion

The table 2 summarizes the experimental and numerical tendencies. This table show similar tendency concerning the inf uence of abrasive size. Therefore, the numerical and the experimental inf uences of tool velocity seem to be in contradiction. A possible explanation is that the numerical model of the f uid is too simple. Probably, during the grinding, lift phenomena could happen. If the tool velocity increases, the lift force may increase also and could affect the effect of the normal pressure. The interactions between f uid and silica could be improved by using more realistic f uid model. A possible way is to couple the DEM model to mesh-free description of f uid like the Smoothed Particle Hydrodynamics (SPH) method [26].

Concerning the abrasive concentration, only the decreasing effect is numerically observed. A global explanation of these divergences is that the parameters, at the macroscopic scale (experimental) could be coupled. For example, the velocity could affect the pressure, and the concentration could affect the relative velocity between tool and silica part.

The table 3 shows a detailed view of numerical results. This table shows the maximal SSD length, the Rough Mean Square (RMS) roughness and the ratio between this two parameters. The maximal SSD values show accordance with those observed in [25]. In addition, if the "velocity -" numerical experience is excluded, it is observed that the ratio is quite stable (around 1.5-1.9). This proportionality between roughness and maximal SSD length has been experimentally observed [27]. This empirical law is intensively exploited to do non-destructive measures of SSD.

Parameter		Maximal SSD length Exp.	Maximal SSD length Dem.
Abrasive size	↗	↗	↗
Tool velocity	↗	↘	↗
Abrasive concentration	↗	↗↘	↘

TABLE 2: Experimental and numerical tendency

Exp. name	$c_{90\%}$ $c_{90\%}$ μm	Roughness rms μm	Ratio $c_{90\%}/rms$
reference	17	10.5	1.6
velocity -	7	9	0.77
velocity +	18	9.5	1.9
radius -	11	7.5	1.5
radius +	22	13	1.7
concentration +	14	8.5	1.6
concentration ++	14	9	1.5

TABLE 3: Detail of numerical results

Conclusion

The presented work used a discrete element model to investigate the sub-surface damage due to loose abrasive grinding. Original numerical methods has been developed to f nely characterize the abraded surface and sub surface damage layer. The numerical results show agreement with some experimentally observed tendencies. Additionally, the maximal SSD length has the same order of magnitude as those observed experimentally. Finally, the empirical between maximal SSD length and roughness has been regained. Therefore some efforts must be done to model more precisely the abrasion interface and, particularly, the f uid interaction by using more realistic f uid model like SPH method.

Acknowledgements

This work is supported by the Conseil Régional d'Aquitaine and is performed in the framework of the Etude et Formation en Surfacage Optique (EFESO) project. The developments carried out during this project have been implemented in the GranOO project. See http://www.granoo.org for details.

REFERENCES

[1] A. J. Glass and A. H. Guenther. Laser induced damage of optical elements—a status report. *Appl. Opt.*, 12(4):637–649, Apr 1973.

[2] D. W. Camp, M. R. Kozlowski, L. M. Sheehan, M. A. Nichols, M. Dovik, R. G. Raether, and I. M. Thomas. Subsurface damage and polishing compound affect the 355-nm laser damage threshold of fused silica surfaces. In *Society of Photo-Optical Instrumentation Engineers (SPIE) Conference Series*, volume 3244 of *Society of Photo-Optical Instrumentation Engineers (SPIE) Conference Series*, pages 356–364, April 1998.

[3] A. Salleo, F. Y. Genin, J. Yoshiyama, C. J. Stolz, and M. R. Kozlowski. Laser-induced damage of fused silica at 355 nm initiated at scratches. In *Society of Photo-Optical Instrumentation Engineers (SPIE) Conference Series*, volume 3244 of *Society of Photo-Optical Instrumentation Engineers (SPIE) Conference Series*, pages 341–347, April 1998.

[4] F. Y. Génin, A. Salleo, T. V. Pistor, and L. L. Chase. Role of light intensif cation by cracks in optical breakdown on surfaces. *J. Opt. Soc. Am. A*, 18(10):2607–2616, Oct 2001.

[5] M. D. Feit and A. M. Rubenchik. Inf uence of subsurface cracks on laser-induced surface damage. In G. J. Exarhos, A. H. Guenther, N. Kaiser, K. L. Lewis, M. J. Soileau, & C. J. Stolz, editor, *Society of Photo-Optical Instrumentation Engineers (SPIE) Conference Series*, volume 5273 of *Society of Photo-Optical Instrumentation Engineers (SPIE) Conference Series*, pages 264–272, June 2004.

[6] H. Bercegol, P. Grua, D. Hébert, and J.-P. Morreeuw. Progress in the understanding of fracture related laser damage of fused silica. In *Proceedings of SPIE*, volume 6720, pages 672003–1. SPIE, 2007.

[7] P. E. Miller, T. Suratwala, J. D. Bude, T. A. Laurence, N. Shen, W. A. Steele, M. Feit, J. Menapace, and L. Wong. Laser damage precursors in fused silica. In *Society of Photo-Optical Instrumentation Engineers (SPIE) Conference Series*, volume 7504 of *Society of Photo-Optical Instrumentation Engineers (SPIE) Conference Series*, October 2009.

[8] I. Iordanoff, B. Seve, and Y. Berthier. Solid third body analysis using a discrete approach: Inf uence of adhesion and particle size on macroscopic properties. *Journal of Tribology*, 124(3):530–538, 2002.

[9] I. Iordanoff and M. M. Khonsari. Granular lubrication: Toward an understanding of the transition between kinetic and quasi-f uid regime. *Journal of Tribology*, 126(1):137–145, 2004.

[10] I. Iordanoff, N. Fillot, and Y. Berthier. Numerical study of a thin layer of cohesive particles under plane shearing. *Powder Technology*, 159(1):46–54, 2005.

[11] N. Fillot, I. Iordanoff, and Y. Berthier. A granular dynamic model for the degradation of material. *Journal of Tribology*, 126(3):606–614, 2004.

[12] N. Fillot, I. Iordanoff, and Y. Berthier. Simulation of wear through mass balance in a dry contact. *Journal of Tribology*, 127(1):230–237, 2005.

[13] D. Richard, I. Iordanoff, Y. Berthier, M. Renouf, and N. Fillot. Friction coeff cient as a macroscopic view of local dissipation. *Journal of Tribology*, 129(4):829–835, 2007.

[14] N. Fillot, I. Iordanoff, and Y. Berthier. Modelling third body f ows with a discrete element method–a tool for understanding wear with adhesive particles. *Tribology International*, 40(6):973–981, 2007. Numerical Simulation Methods in Tribology: possibilities and limitations.

[15] I. Iordanoff, A. Battentier, J. Neauport, and J.L. Charles. A discrete element model to investigate sub-surface damage due to surface polishing. *Tribology International*, 41(11):957–964, 2008.

[16] E. Rougier, A. Munjiza, and N. W. M. John. Numerical comparison of some explicit time integration schemes used in dem, fem/dem and molecular dynamics. *International Journal for Numerical Methods in Engineering*, 61(6):856–879, 2004.

[17] D. Eberly. *Game physics*. Elsevier, Morgan Kaufmann, 30 Corporate Drive, Suite 400, Burlington, MA 01803 USA, second edition edition, 2010.

[18] T. Pöschel and T. Schwager. *Computational granular dynamics*. Springer, 2005.

[19] E. Schlangen and E.J. Garboczi. Fracture simulations of concrete using lattice models: Computational aspects. *Engineering Fracture Mechanics*, 57(2-3):319–332, 1997.

[20] E. Schlangen and E. J. Garboczi. New method for simulating fracture using an elastically uniform random geometry lattice. *International Journal of Engineering Science*, 34(10):1131–1144, 1996.

[21] S. P. Timoshenko. *History of strength of materials: with a brief account of the history of theory of elasticity and theory of structures*. Dover, New York, NY.

[22] O. G. Gupta. *Finite and boundary element methods in engineering*. Belkema, A. A., 1999.

[23] J. Happel and H. Brenner. *Low Reynolds number hydrodynamics: with special applications to particulate media*. Mechanics of f uids and transport processes. M. Nijhoff, 1983.

[24] T. Suratwala, P. Davis, L. Wong, P. Miller, M. Feit, J. Menapace, R. Steele, and D. Walmer. Sub-surface mechanical damage distributions during grinding of fused silica. *Journal of Non-Crystalline Solids*, 352:5601–5617, 2006.

[25] J. Neauport, J. Destribats, C. Maunier, C. Ambard, P. Cormont, B. Pintault, and O. Rondeau. Loose abrasive slurries for optical glass lapping. *Appl. Opt.*, 49(30):5736–5745, Oct 2010.

[26] G. R. Liu and M. B. Liu. *Smoothed particle hydrodynam-*

ics: a meshfree particle method. World Scientif c, 2003.

[27] J. Neauport, C. Ambard, P. Cormont, N. Darbois, J. Destribats, C. Luitot, and O. Rondeau. Subsurface damage measurement of ground fused silica parts by hf etching techniques. *Opt. Express*, 17(22):20448–20456, Oct 2009.